Pergamon

Int. J. Solids Structures Vol. 34, Nos. 35–36, pp. 4531–4546, 1997

0020–7683/97 $17.00 + .00

PII: S0020–7683(97)00039–5

POST-NECKING BEHAVIOUR MODELLED BY A GRADIENT DEPENDENT PLASTICITY THEORY

LARS PILGAARD MIKKELSEN
Department of Solid Mechanics, Technical University of Denmark, DK-2800 Lyngby, Denmark

(*Received* 13 *August* 1996; *in revised form* 14 *January* 1997)

Abstract—The delay of the onset of localization and the post-necking behaviour for stretched thin sheets are determined by three-dimensional effects. Thus, a 2-D finite element analysis based on a local plasticity theory will give a physically unrealistic mesh dependent solution. This, in spite of the fact that the stress state, is essentially two-dimensional. By incorporating a length scale with relation to the thickness of the sheet, it is demonstrated how a 2-D finite element analysis based on a gradient dependent plasticity theory can give a good approximation of the post-necking behaviour. This is illustrated by numerical comparison of results from a full 3-D finite element analysis, with results from a 2-D finite element model based on a finite strain version of a gradient dependent J_2-flow theory. Some numerical problems in the modeling will be discussed briefly. © 1997 Elsevier Science Ltd.

1. INTRODUCTION

A detailed understanding of the necking and post-necking behaviour of biaxially stretched sheets is highly relevant during sheet metal forming, Keeler (1968). This is due to the fact that the necking point specifies the forming limit of the sheet metal and the width of the necking zone specifies the ductility of the post failure behaviour. Necking in a sheet develops after the onset of localization of the deformation pattern. Both the delay of the onset of localization and the post-necking behaviour of an imperfect thin sheet are determined by three-dimensional (3-D) effects. An accurate finite element analysis based on a classical (local) plasticity theory is, therefore, restricted to a full 3-D model, Tvergaard (1993). The corresponding two-dimensional (2-D) finite element analysis will give a physically unrealistic mesh sensitive solution, where the necking zone occupies the smallest possible area allowed for by the mesh.

A way to remedy the spurious mesh sensitivity is to incorporate an internal length scale into the material description. Thereby, it is possible to obtain a mesh independent post-necking behaviour for the stretched sheet by using a 2-D plane stress finite element model. An evaluation of the applicability of these mesh independent 2-D solutions to model the real post-necking behaviour can be evaluated by comparison with the full 3-D finite element solution found with the corresponding classical plasticity theory. A similar comparison can be made between a 2-D (plane strain in the direction of the width of the specimen) classical plasticity model and a one-dimensional (1-D) (plane strain in the direction of the width and plane stress in the direction of the thickness) strain gradient dependent model. Such comparisons are the aim of the present paper.

Several different ways to incorporate an internal length scale into the material description have been proposed in the literature. The Cosserat (micropolar) continuum model (Eringen, 1968; Mühlhaus and Vardoulakis, 1987; Fleck and Hutchinson, 1993) introduces the length scale by an additional degree-of-freedom (microrotation). In the Cosserat theory these additional degrees-of-freedom are activated during the deformation, i.e. in shear dominated problems. For pure tension problems the effect is reduced significantly due to small curvatures within the localization band (Pamin, 1994; Fleck and Hutchinson, 1996). Models which incorporate a strengthening effect due to the first or second Laplacian of the effective strain (gradient dependent theories) (Aifantis, 1984; Aifantis, 1987; Mühlhaus and Aifantis, 1991; de Borst and Mühlhaus, 1992) have shown to be more convenient for

tension dominated problems, which is also the case for non-local integral models [see for example Pijaudier-Cabot and Bazant (1987)].

Non-local models have mainly been used to remedy the mesh sensitivity in softening materials, where the softening mechanism depends on the microstructure. For ductile metals the relevant length scale is e.g. dislocation cell sizes, reinforcing particle diameters, void spacings or grain sizes. For the necking behaviour of stretched sheet metal the material itself is hardening and the overall softening is, thus, due purely to geometric effects caused by a variation in the instantaneous thickness of the sheet. This effect is incorporated in the model by a finite strain theory. For the necking case the relevant length is of the order of the thickness of the stretched sheet, see Benallal and Tvergaard (1995).

In this work, a finite strain version of the gradient dependent plasticity theory proposed by de Borst and Mühlhaus (1992) is used, similar to the model used by Benallal and Tvergaard (1995). The gradient dependence is incorporated in the yield condition by a dependence not only on the effective plastic strain, but also on the Laplacian thereof. The dependence on the Laplacian of the effective strain results in a strengthening of the material in the middle of a localization band (an increase of the instantaneously yield stress), as well as a softening of the material at the boundaries of the band (a decrease of the instantaneously yield stress). This forces the localization zone to spread. Thus, a gradient dependent yield condition incorporates a length scale in the material behaviour.

The non-local plasticity theory is incorporated in a finite element method, where the effective plastic strain and its gradients, are considered as fundamental unknowns having a role similar to that of the displacements. When the Laplacian of the effective plastic strain is taken with respect to the undeformed reference state, the increment of the displacements can be modelled by 8-noded isoparametric element, while the effective plastic strain is modelled by Hermitian cubics (due to the second derivative). If, alternatively, the Laplacian of the effective plastic strain is taken with respect to the current deformed state, second-order derivatives of the displacements appear in the governing equations. Therefore, in this alternative formulation, both the increment of the plastic strain and the displacements must be modelled by Hermitian cubics (C^1-compatibility). This gives rise to some numerical difficulties which will be discussed briefly in Section 5.4.

2. CLASSICAL J_2-FLOW THEORY

The finite strain theory used is a standard Lagrangian convected coordinate formulation [see for example Budiansky (1969) or Hutchinson (1973)], which will be outlined briefly in the following. The covariant components of the metric tensor of the undeformed and the deformed configurations are denoted g_{ij} and G_{ij}, respectively. A Cartesian reference coordinate system is chosen in the undeformed configuration. General tensor notation is adopted. Upper and lower indices denote the contravariant and the covariant components of the tensors, respectively. Repeated indices mean summation, where Latin indices range from 1 to 3 while Greek indices range from one to two. Covariants differentiation is written $(\,)_{|i}$, while the increments are denoted $\dot{(\,)}$. The increments of the Lagrangian strain $\eta_{ij} = 1/2(G_{ij} - g_{ij})$ are given by

$$\dot{\eta}_{ij} = \tfrac{1}{2}(\dot{u}_{i|j} + \dot{u}_{j|i} + \dot{u}^k_{|i} u_{k|j} + u^k_{|i} \dot{u}_{k|j}). \tag{1}$$

The total strain increment $\dot{\eta}_{ij}$ is taken as the sum of an elastic part $\dot{\eta}^{\mathrm{E}}_{ij}$ and a plastic part $\dot{\eta}^{\mathrm{P}}_{ij}$. Thus, the constitutive law is written as

$$\overset{\nabla}{\sigma}{}^{ij} = \mathscr{L}^{ijkl}(\dot{\eta}_{kl} - \dot{\eta}^{\mathrm{P}}_{kl}) \tag{2}$$

where $\overset{\nabla}{\sigma}{}^{ij}$ is the Jaumann derivative of the Cauchy stress and the elastic moduli are

$$\mathscr{L}^{ijkl} = \frac{E}{1+\nu}\{\tfrac{1}{2}(G^{ik}G^{jl}+G^{il}G^{jk}) + \frac{\nu}{1-2\nu}G^{ij}G^{kl}\} \tag{3}$$

with Young's modulus, E, and Poisson's ratio, ν. The Jaumann derivative of the Cauchy stress is related to the convected derivative by

$$\overset{\nabla}{\sigma}{}^{ij} = \dot{\sigma}^{ij} + (G^{ik}\sigma^{jl} + G^{jk}\sigma^{il})\dot{\eta}_{kl}. \tag{4}$$

The von Mises yield surface is

$$f = \sigma_e(\sigma^{ij}) - \sigma_y(\varepsilon_e^{\mathrm{P}}) \leqslant 0 \tag{5}$$

where the von Mises stress $\sigma_e = (3s^{ij}s_{ij}/2)^{1/2}$ depends on the stress deviator

$$s^{ij} = \sigma^{ij} - G^{ij}\sigma_k^k/3,$$

with

$$\sigma_k^k = G_{kl}\sigma^{kl}.$$

The instantaneous yield stress is modelled by a power law

$$\sigma_y(\varepsilon_e^{\mathrm{P}}) = \sigma_0(1 + \frac{E}{\sigma_0}\varepsilon_e^{\mathrm{P}})^{1/n} \tag{6}$$

with the strain hardening exponent n, the initial yield stress σ_0, and the effective plastic strain is given through its increments

$$\dot{\varepsilon}_e^{\mathrm{P}} = (2\dot{\eta}_{ij}^{\mathrm{P}}\dot{\eta}_{\mathrm{P}}^{ij}/3)^{1/2}.$$

From the requirement of normality of the plastic strain increment $\dot{\eta}_{ij}^{\mathrm{P}}$ relative to the yield surface f, the plastic strain increment is given by

$$\dot{\eta}_{ij}^{\mathrm{P}} = \dot{\lambda}m_{ij}, \quad m_{ij} = \frac{\partial f}{\partial \sigma^{ij}} = \frac{3s_{ij}}{2\sigma_e} \tag{7}$$

where $\dot{\lambda}$ is the increment of the plastic multiplier. From the definition

$$\dot{\varepsilon}_e^{\mathrm{P}} = (2\dot{\eta}_{ij}^{\mathrm{P}}\dot{\eta}_{\mathrm{P}}^{ij}/3)^{1/2}$$

it follows that $\dot{\lambda} = \dot{\varepsilon}_e^{\mathrm{P}}$.

For a classical local plasticity theory the increment of the plastic multiplier is explicitly given by the consistency condition, $\dot{f} = 0$, which is found from eqn (5) as

$$\dot{f} = m_{ij}\overset{\nabla}{\sigma}{}^{ij} + h(\lambda)\dot{\lambda} = 0 \tag{8}$$

with m_{ij} given by (7) and $h(\lambda) = \partial f/\partial\lambda$. The identity $\lambda = \varepsilon_e^{\mathrm{P}}$, which follows from $\dot{\lambda} = \dot{\varepsilon}_e^{\mathrm{P}}$, is used.

A numerical solution is carried out by a finite element analysis based on the principle of virtual work on incremental form

$$\int_v \{\dot{\sigma}^{ij}\delta\eta_{ij}+\sigma^{ii}\dot{u}_{k,j}\delta u^k_{,i}\}\,\mathrm{d}V = \int_S \dot{T}^i\delta u_i\,\mathrm{d}S-\left[\int_V \sigma^{ii}\delta\eta_{ij}\,\mathrm{d}V-\int_S T^i\delta u_i\,\mathrm{d}S\right] \tag{9}$$

where V and S are the reference volume and surface of the region analyzed, and T^i are the specified nominal surface tractions. In the expression for the virtual work (9), the Kirchhoff stress τ^{ij} has been replaced by the Cauchy stress, as the approximation $\tau^{ij} \approx \sigma^{ij}$ is reasonable as long as the elastic strains are small (Hutchinson, 1973). The bracketed terms are introduced to avoid drifting away from the equilibrium path.

3. GRADIENT DEPENDENT J_2-FLOW THEORY

The gradient dependent von Mises yield surface

$$f = \sigma_e(\sigma^{ij})-\tilde{\sigma}_y(\lambda,\nabla^2\lambda) \leqslant 0 \tag{10}$$

differs from the classical von Mises yield surface (5) by an instantaneous yield stress $\tilde{\sigma}_y$ which depends both on the plastic multiplier λ and its Laplacian. The gradient dependent yield stress is modelled by a linear dependence on $\nabla_0^2\lambda$.

$$\tilde{\sigma}_y(\lambda,\nabla^2\lambda) = \sigma_y(\lambda)-g(\lambda)\nabla_0^2\lambda \tag{11}$$

through the gradient influence function $g(\lambda)$ (Pamin, 1994; Pamin and de Borst, 1995), which is a generalization of the gradient dependent yield stress applied in the paper by de Borst and Mühlhaus (1992). It is assumed that $\tilde{\sigma}_y > 0$. The Laplacian of the plastic multiplier is here chosen to be taken with respect to the Cartesian reference state $\nabla_0^2\lambda = \lambda_{,ii}$, where $(\,)_{,i}$ denotes the partial derivative with respect to the convected coordinates x^i. An alternative is to take the Laplacian with respect to the current deformation state $\nabla^2\lambda = (G^{ij}\lambda_{,i})_{,j}$ (Spiegel, 1959). This alternative Laplacian is discussed in a later section (Section 5.4). For a positive $g(\lambda)$, eqn (11) results in a higher instantaneous yield stress for $\nabla_0^2\lambda < 0$, while the instantaneous yield stress will be reduced for $\nabla_0^2\lambda > 0$. This effect will force the localization zone to spread as $\nabla_0^2\lambda > 0$ in the middle of the localized band, while $\nabla_0^2\lambda > 0$ on the boundaries of the localization band. The function $g(\lambda)$ can be modelled rather arbitrary, just to obtain the wanted non-local effect. For softening materials Pamin (1994) and Pamin and de Borst (1995) have suggested $g(\lambda) = -\ell^2\mathrm{d}\sigma_y/\mathrm{d}\lambda$ which is a generalization of the case for linear softening, where $\mathrm{d}\sigma_y/\mathrm{d}\lambda < 0$. Here, ℓ is an internal length scale. In the present work, the non-local effects are not due to micro-mechanical effects, but rather due to purely geometric effects caused by the necking of the sheet. Later in Section 5.2 different choices of the function $g(\lambda)$ are discussed. For an internal length scale $\ell = 0$ the gradient dependency vanishes and the yield stress (11) coincides with the classical von Mises yield stress (5).

Contrary to a classical plasticity theory, where the increment of the plastic multiplier is explicitly given from the consistency condition (8), this is not the case for a gradient dependent plasticity theory. In this case, the consistency condition takes the form

$$\dot{f} = m_{ij}\overset{\nabla}{\sigma}{}^{ij}+h(\lambda,\nabla_0^2\lambda)\dot{\lambda}+g(\lambda)(\nabla_0^2\lambda)^{\cdot} = 0 \tag{12}$$

where $\dot{\lambda}$ and $(\nabla_0^2\lambda)^{\cdot}$ is treated as two independent variables. Analogous to the virtual work on incremental form (9), the consistency condition (12), which now is a differential equation in $\dot{\lambda}$, can be solved by a weak formulation

$$\int_{V_\lambda} \dot{f}\delta\dot{\lambda}\,\mathrm{d}V_\lambda = \left[\int_{V_\lambda} f\delta\dot{\lambda}\,\mathrm{d}V_\lambda\right] \tag{13}$$

where V_λ is the volume of the current plastic zone in the structure. The bracketed term is introduced to avoid the solution to drift away from the yield surface.

4. THE NUMERICAL MODEL

The stress state in the thin sheet is assumed to be approximately plane ($\sigma^{i3} = \sigma^{3i} = 0$), and all the variable can be taken to be constant in the x^3-direction, equal to their values in the middle surface. Thus, the strains $\eta_{\alpha 3} = \eta_{3\alpha} = 0$. With these approximations, the virtual work on incremental form (9) and the weak formulation of the consistency condition (13) can be written as

$$\int_A \left\{\left(\hat{L}^{\alpha\beta\gamma\delta}\dot{\eta}_{\gamma\delta} - \hat{\mathscr{L}}^{\alpha\beta\gamma\delta}\dot{\lambda}m_{\gamma\delta}\right)\delta\dot{\eta}_{\alpha\beta} + \sigma^{\alpha\beta}\dot{u}_{\gamma,\beta}\delta\dot{u}^{\gamma}_{,\alpha}\right\} 2\bar{H}_0\,\mathrm{d}A$$
$$= \int_S \dot{T}^\alpha \delta\dot{u}_\alpha\,\mathrm{d}S - \left[\int_A \sigma^{\alpha\beta}\delta\dot{\eta}_{\alpha\beta}2\bar{H}_0\,\mathrm{d}A - \int_S T^\alpha\delta\dot{u}_\alpha\,\mathrm{d}S\right] \tag{14}$$

and

$$\int_{A_\lambda} \left\{-m_{\alpha\beta}\hat{\mathscr{L}}^{\alpha\beta\gamma\delta}\dot{\eta}_{\gamma\delta} + \left(m_{\alpha\beta}\hat{\mathscr{L}}^{\alpha\beta\gamma\delta}m_{\gamma\delta} - h(\lambda, \nabla_0^2\lambda)\right)\dot{\lambda} + g(\lambda)(\nabla_0^2\lambda)^{\cdot}\right\}\delta\dot{\lambda}2\bar{H}_0\,\mathrm{d}A_\lambda$$
$$= \left[\int_{A_\lambda} f\delta\dot{\lambda}2\bar{H}_0\,\mathrm{d}A_\lambda\right] \tag{15}$$

with the thickness function $2\bar{H}_0$ and where the plane stress instantaneous moduli is given by

$$\hat{L}^{\alpha\beta\gamma\delta} = L^{\alpha\beta\gamma\delta} - \frac{L^{\alpha\beta 33}L^{33\gamma\delta}}{L^{3333}}, \quad \hat{\mathscr{L}}^{\alpha\beta\gamma\delta} = \mathscr{L}^{\alpha\beta\gamma\delta} - \frac{\mathscr{L}^{\alpha\beta 33}\mathscr{L}^{33\gamma\delta}}{\mathscr{L}^{3333}}. \tag{16}$$

Here $\mathscr{L}^{ijkl}$ is given by eqn (3) and L^{ijkl} is found from (4) to be

$$L^{ijkl} = \mathscr{L}^{ijkl} - \tfrac{1}{2}(G^{ik}\sigma^{jl} + G^{jk}\sigma^{il} + G^{il}\sigma^{jk} + G^{jl}\sigma^{ik}). \tag{17}$$

In the numerical solution the area A_λ is replaced by A. This is reasonable if the elastic part of the structure is modelled with $h(\lambda, \nabla_0^2\lambda)$ equal to a large number (e.g. $h = 10^{10}E$) and with $f = 0$. The area A is discretised into a rectangular finite element mesh where the integrals in eqns (14) and (15) are evaluated by a 2×2 Gauss integration. For a corresponding 3×3 Gauss integration scheme some oscillations of the yield function f between the integrations points have been observed (see also Pamin, 1994). The displacement increment $\dot{u}_\alpha$ is modelled by an 8-noded isoparametric element, while the increment of the plastic multiplier $\dot{\lambda}$ is modelled by a 4-noded Hermitian element (Hermitian cubics). Due to the Hermitian shape function, which is introduced to satisfy the requirement of a C^1-continuous shape function for $\dot{\lambda}$, the element is constrained to be rectangular. As in Mühlhaus and Aifantis (1991) and Benallal and Tvergaard (1995) the non-standard boundary condition

$$\dot{\lambda} = 0 \quad \text{or} \quad \frac{\partial\dot{\lambda}}{\partial\mathbf{n}} = 0 \tag{18}$$

is introduced on the boundary of the structure, where $\mathbf{n}$ is the outwards normal.

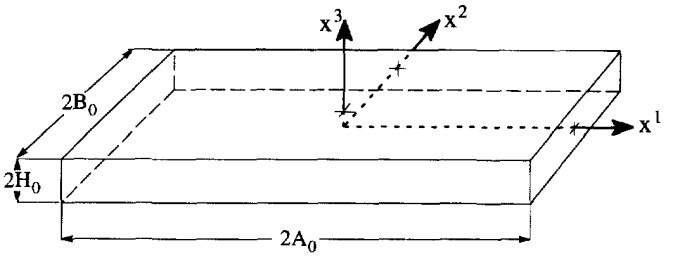

Fig. 1. Rectangular tensile test specimen.

For each increment the stress components $\sigma^{\alpha\beta}$ and the value G_{33} in the Gauss integration points, as well as the displacements and the plastic multiplier in the nodes, are updated by a linear Euler integration based on the material condition in the previous increment. Plastic yielding occurs when $f > 0$, while elastic unloading takes place when $\dot{\lambda} < 0$. In the case with plastic unloading and $f > 0$, yielding occurs again when $\dot{\sigma}_e > 0$. In the few increments where $\lambda < 0$, $\dot{\lambda}$ is constrained to be zero in the updating procedure. The requirement $f = 0$ for plastic yielding is in the numerical procedure taken to be satisfied of $f \leqslant 10^{-3}\sigma_0$.

The applicability of the gradient dependent plasticity theory for describing the post-necking behaviour is investigated in numerical analyses for a rectangular tensile test specimen (Fig. 1). The gradient dependent analysis is compared to an accurate full numerical analysis based on a classical plasticity theory. The evaluation of the capability of the gradient dependent models as an approach to the real post-necking behaviour is based on three criteria: (1) the prediction of the delay of the onset of localization compared to the maximum load (Hill and Hutchinson, 1975); (2) the prediction of the load deflection curve in the post-necking zone; (3) a correct deformation state (i.e. the thickness variation or the variation of the maximum principal strain) in the specimen.

The geometry of the specimen (Fig. 1) is specified by the initial length $2A_0$, the initial width $2B_0$ and the initial thickness $2\bar{H}_0$, in the x^1, x^2 and x^3 direction, respectively. The necking behaviour of the test specimen is initiated by a small imperfection in the thickness

$$\bar{H}_0(x^1, x^2) = H_0\left(1 - \bar{\xi}\cos\frac{\pi x^*}{A_0}\right), \quad x^* = x^1 + x^2\tan(\phi) \tag{19}$$

where $\bar{\xi}$ is the imperfection amplitude and ϕ the inclination angle with respect to the x^2-axis [see also Tvergaard (1993)]. The tension of the specimen is specified by an average logarithmic strain $\varepsilon_a = \ln(1 + U/A_0)$, where U is the displacement at both ends. The corresponding average nominal traction in the axial direction is denoted T_a.

5. NUMERICAL RESULTS

5.1. *Results for the 1-D gradient dependent model*

The non-local effect of the gradient dependent plasticity theory is demonstrated in Fig. 2(a, b). A slender tensile test specimen ($A_0/H_0 = 100$) is analyzed, where the material is given by $\sigma_0/E = 0.001$, $n = 10$ and $\nu = 0.3$. The amplitude $g(\lambda)$ of the gradient dependence in (11) is here chosen to be a constant $g(\lambda) = \ell^2\sigma_0$. Here, the parameter ℓ with dimension length is not a uniquely defined material length, but it can be used as the incorporated length [see for example de Borst and Mühlhaus (1992)].

In the problems considered here, the contraction in the x^2-direction is constrained to be equal to zero. Thus, it is essentially a 1-D numerical problem (plane stress in the x^3-direction and plane strain in the x^2-direction) where the necking zone is orthogonal to the axial direction [e.g. Tvergaard (1981)]. One row of elements in the axial direction is therefore sufficient in the numerical analysis. The imperfection of the sheet thickness is specified by the amplitude $\bar{\xi} = 0.001$ and no inclination $\phi = 0$ (19). Only one half of the specimen ($0 < x^1 < A_0$) is analyzed, with symmetry boundary conditions for $x^1 = 0$.

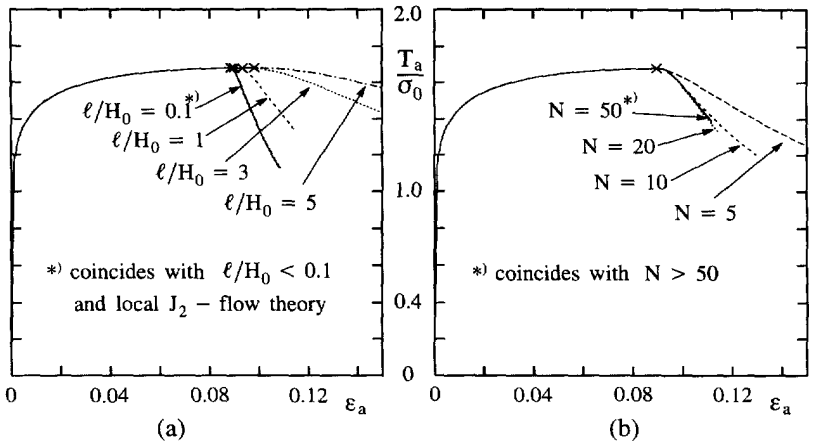

Fig. 2. The average nominal traction versus average longitudinal strain for a specimen with $A_0/H_0 = 100$, $\bar{\xi} = 0.001$, $\phi = 0$, $\sigma_0/E = 0.001$, $n = 10$, $\nu = 0.3$ and $g(\lambda) = \ell^2\sigma_0$ for (a) $N = 20$ equidistant elements in the longitudinal direction and (b) an incorporated length $\ell = H_0$.

In Fig. 2(a) the effects of the size of the incorporated length scale for a fixed mesh (20 equidistant elements in the axial direction) are compared to the corresponding local plasticity theory. It is seen how a sufficiently large length scale ℓ gives a stiffer response (higher loads for a given tension) of the post-necking behaviour with a delay of the onset of localization. This is defined as the point on the load deflection curve where the first integration point shows elastic unloading (mark on the curves). For a sufficiently small length ℓ the post-necking behaviour is seen to coincide with the solution for the local plasticity theory. This is due to the fact that the length scale in the structure is no longer given by the gradient dependent constitutive law, but by the element size. The load vs strain curves are in all the calculations (except for the 2-D gradient dependent analysis, Figs 8, 7 and 10) stopped when the current thickness in one of the integration points reaches $H \leqslant H_0/2$.

The effect of different finite element mesh refinement for a fixed value of the length ℓ are shown in Fig. 2(b). It is seen how a sufficiently fine mesh gives a mesh independent solution ($N > 50$). That will not be the case for a local plasticity model where the deformation state after the onset of localization will always be concentrated in the smallest possible area, which corresponds to 1–2 elements in the numerical model. Thus, a local plasticity model will tend to give a physically unrealistic mesh dependent solution.

5.2. *The gradient dependent model (1-D) compared to the full plane strain local model (2-D)*

Figure 3 shows a comparison between a 1-D (plane strain plane stress) gradient dependent analysis (dashed curves), a 1-D classical analysis (dotted curves) and an accurate full 2-D (plane strain) classical analysis (solid curve). In the full 2-D numerical model, the imperfection (19) has been implemented by perturbing the thickness of the surface layer of elements (by a factor between 1.001 and 0.999 for $\bar{\xi} = 0.001$). In the gradient dependent model the delay of the onset of localization is governed by the incorporated length scale (Mikkelsen, 1996). In Fig. 3 the length ℓ is chosen such that the onset of localization for the gradient dependent model coincide with the corresponding onset of localization for the accurate model. Results are shown for two different gradient influence functions ($g(\lambda) = \ell^2\sigma_y(\lambda)$, $g(\lambda) = \ell^2\sigma_0$) and for an incorporated length scale which is normalized with respect to either the initial thickness ($\ell/H_0 = \alpha_0$) or the current thickness in the integration point ($\ell/H_c = \alpha_c$). The two parameters α_0 and α_c are treated as constants. In the finite element analysis for one half of the specimen ($0 < x^1 < A_0$), it suffices with 30×10 elements for the 2-D model and 30×1 for the gradient dependent 1-D model, with a concentration of the elements in the necking zone in the axial direction (similar to the mesh shown in Fig. 6(a)). This has been estimated based on a few calculations with finer meshes. On the other hand, the 1-D classical analysis (dotted curve) results in a highly mesh sensitive post-necking behaviour. For comparison, solutions for 10×1, 3×1 and 2×1 elements are

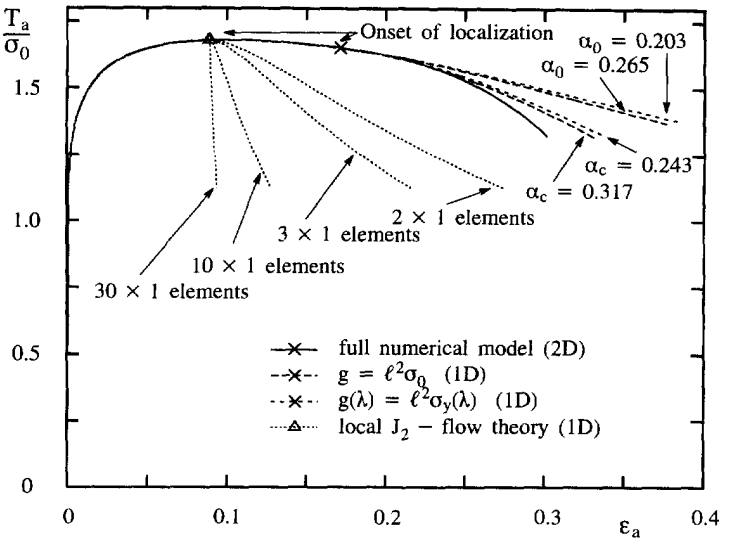

Fig. 3. The average nominal traction versus the average longitudinal strain for a stocky specimen with $A_0/H_0 = 2$, $\bar{\xi} = 0.001$, $\phi = 0$, $\sigma_0/E = 0.001$, $n = 10$ and $\nu = 0.3$. The incorporated length scale is given with either $\ell = \alpha_c H$ or $\ell = \alpha_0 H_0$.

shown. Even for the very coarse mesh (2 × 1 elements) the post-necking behaviour obtained is very soft with a vanishing delay of the onset of localization (compared with the maximum load point).

In Fig. 3 only a minor difference is observed in the post-necking behaviour for the two gradient influence functions. The function $g(\lambda) = \ell^2\sigma_y(\lambda)$ gives a slightly stiffer post-necking response than that predicted for $g(\lambda) = \ell^2\sigma_0$. This is due to the fact, that for a hardening material (6) $\sigma_y(\lambda)$ is growing compared to σ_0. For some problems with softening, i.e. $d\sigma_y/d\lambda < 0$, Pamin and de Borst (1995) have used the gradient influence function $g(\lambda) = -\ell^2 d\sigma_y/d\lambda$, but this is not relevant to the present case.

A significantly larger difference in the post-necking behaviour is obtained if the incorporated length scale in the gradient dependent model is normalized with respect to the current thickness in the integration point ($\ell = \alpha_c H$) instead of a normalization with respect to the initial thickness ($\ell = \alpha_0 H_0$), but as can be seen in Fig. 3, none of the gradient dependent models show in a sufficiently soft post-necking behaviour. The load is too high for a given strain, compared to the full (2-D) numerical analysis (solid line). This difference could be minimized by reducing the incorporated length scale. That will result in a softer solution, but also in a premature onset of the localization.

Figure 4 shows a comparison of the thickness variation in the axial direction for the gradient dependent model with $g(\lambda) = \ell^2\sigma_y(\lambda)$ where $\ell = 0.243H$, and the corresponding full (2-D) numerical model. Despite the fact that the gradient dependent model (dashed curves) is slightly more localized at the onset of localization, it is seen how the full numerical model is significantly more localized far into the post-necking region (at $\varepsilon_a = 0.26$ and $\varepsilon_a = 0.30$), which would correspond to a decreased incorporated length.

It would be attractive if the difference between the gradient dependent model and the full numerical model was independent of a change in the initial yield stress σ_0 and the hardening exponent n. Compared to Fig. 3, the hardening exponent in Fig. 5(a) is changed from $n = 10$–3, and the initial yield stress in Fig. 5(b) is changed from $\sigma_0/E = 0.001$–0.005. All other values, also the incorporated length, are unchanged. None of the gradient dependent models analyzed are insensitive to a change in the hardening exponent (Fig. 5(a)). On the other hand, the gradient dependent model using $g(\lambda) = \ell^2\sigma_y(\lambda)$ as an approach to the post-necking behaviour, is insensitive to a change of the initial yield stress (Fig. 5(b)).

In Fig. 6 the gradient dependent model with $g(\lambda) = \ell^2\sigma_y(\lambda)$ and $\ell = 0.243H$ is compared to the accurate full numerical model for three different length to thickness ratios. The gradient dependent model is seen to capture the decreased delay of the onset of localization for more slender specimens and the discrepancy of the post-necking path is seen to be of

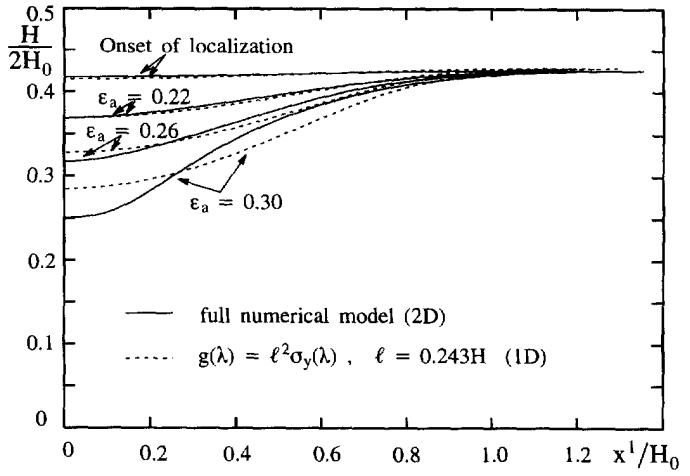

Fig. 4. The thickness variation of the stretched specimen at four different deformation states for the full numerical model (2-D), and one of the gradient dependent calculation for a specimen with $A_0/H_0 = 2$, $\bar{\xi} = 0.001$, $\phi = 0$, $\sigma_0/E = 0.001$, $n = 10$ and $\nu = 0.3$.

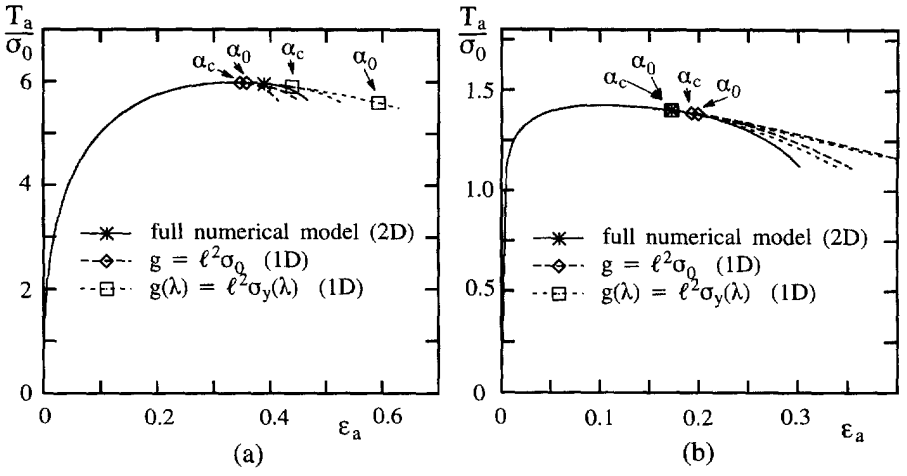

Fig. 5. The average nominal traction versus the average longitudinal strain for a specimen with $A_0/H_0 = 2$, $\bar{\xi} = 0.001$, $\phi = 0$, $\nu = 0.3$ with (a) $\sigma_0/E = 0.001$, $n = 3$ and (b) $\sigma_0/E = 0.005$, $n = 10$. The incorporated length scale is the same as in Fig. 3, given by $\alpha_0 = 0.265$ and $\alpha_c = 0.317$ for $g = \ell^2\sigma_0$ and by $\alpha_0 = 0.203$ and $\alpha_c = 0.243$ for $g(\lambda) = \ell^2\sigma_y(\lambda)$.

the same magnitude for the three length to thickness ratios. For the stocky specimen ($A_0/H_0 = 2$) the deformed mesh and the current zone of plastic yielding is shown for the full numerical model at three points of the loading history (Figs 6(a–c)).

The points for the onset of localization according to the gradient dependent model and the full numerical model are compared in spite of the fact that the full numerical model begins to unload in the middle surface of the specimen (see Fig. 6(a)) while the unloading of an integration point in the gradient dependent model corresponds to an average unloading through the thickness. More correctly, the point for the onset of localization in the gradient dependent model should lie somewhere between the point for the onset of localization ($\times$ in Fig. 6) and the point for unloading through the thickness (+in Fig. 6) for the full numerical model. That is to say, the incorporated length should be chosen slightly larger, which would slightly increase the difference between the gradient dependent model and the full numerical model in the post-necking area.

5.3. *Results for the 2-D gradient dependent model*

The next analysis is for a rectangular tensile bar (Fig. 1) which is free to contract in the x^2-direction. This will result in two competitive necking modes; a diffuse mode, where the length of the necking region in axial direction is of the order of the specimen width,

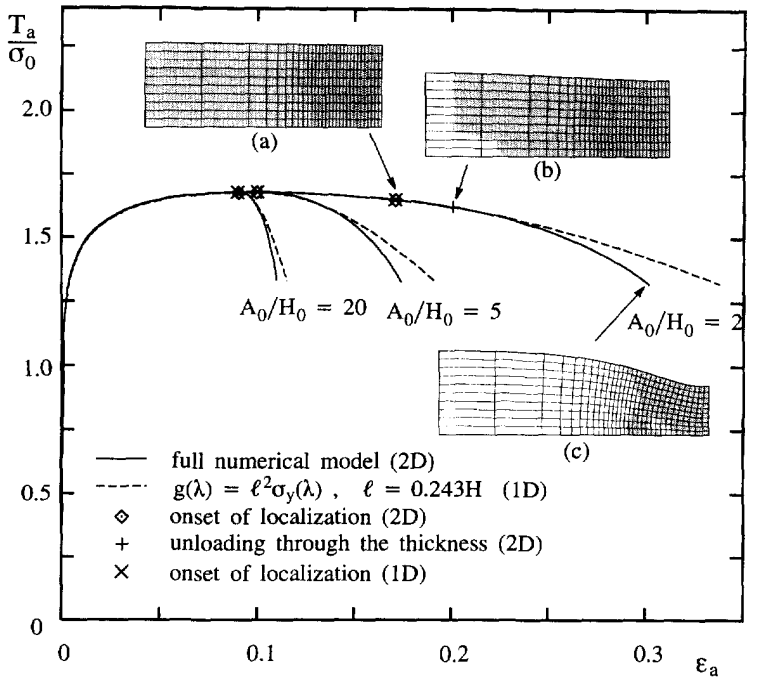

Fig. 6. The average nominal traction versus the average longitudinal strain for a specimen with $A_0/H_0 = 2$, $\bar{\xi} = 0.001$, $\phi = 0$, $\sigma_0/E = 0.001$, $n = 10$ and $\nu = 0.3$. (a–c) Deformed mesh for the full numerical model. (a) At onset of localization; (b) at unloading through the thickness; and (c) final deformed mesh at a thickness reducing $H_{\min} = H_0/2$. The gray zone in the deformed meshes indicate the zone in the specimen where plastic yielding is in progress.

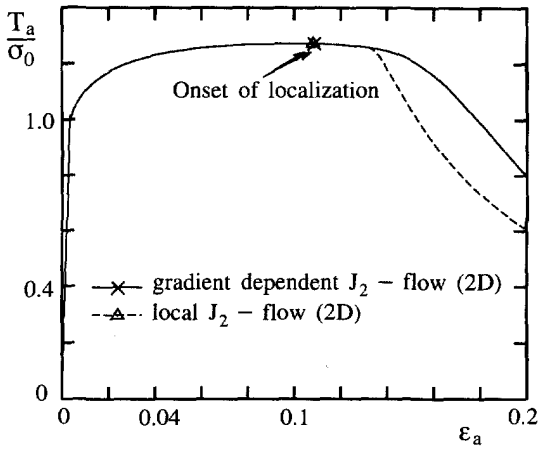

Fig. 7. The average nominal traction vs the average longitudinal strain for a specimen with $A_0/B_0 = 2$, $B_0/H_0 = 16$, $\bar{\xi} = 0.001$, $\phi = 0$, $\sigma_0/E = 0.0033$, $n = 10$ and $\nu = 0.3$. The gradient dependent J_2-flow theory is given by $g(\lambda) = \ell^2\sigma_y(\lambda)$ with $\ell = 0.243H$.

and two crossing oblique localized necks with a width of the order of the specimen thickness, Tvergaard (1993). In cases where no symmetry condition is specified on the centerlines of the uniaxial tensile test specimen, $x^1 = 0$ and $x^2 = 0$ (see Fig. 1), one of the two crossing bands will saturate while the other necking band will grow into the failure mode. Due to the inclination of the necking band, the study must be based on a 2-D gradient dependent finite element analysis, or on a full 3-D local plasticity model (see Tvergaard, 1993).

In Figs 7–8, one-quarter ($-A_0 < x^1 < 0$, $0 < x^2 < B_0$) of the specimen is analysed, with symmetry boundary conditions specified along the two centerlines, $x^1 = 0$ and $x^2 = 0$. Figure 7 compares two 2-D finite element models. A gradient dependent model with the gradient influence function $g(\lambda) = \ell^2\sigma_y(\lambda)$ for $\ell = 0.243H$ and the corresponding local 2-D plasticity model (mesh dependent solution) found for the same mesh. In accordance with

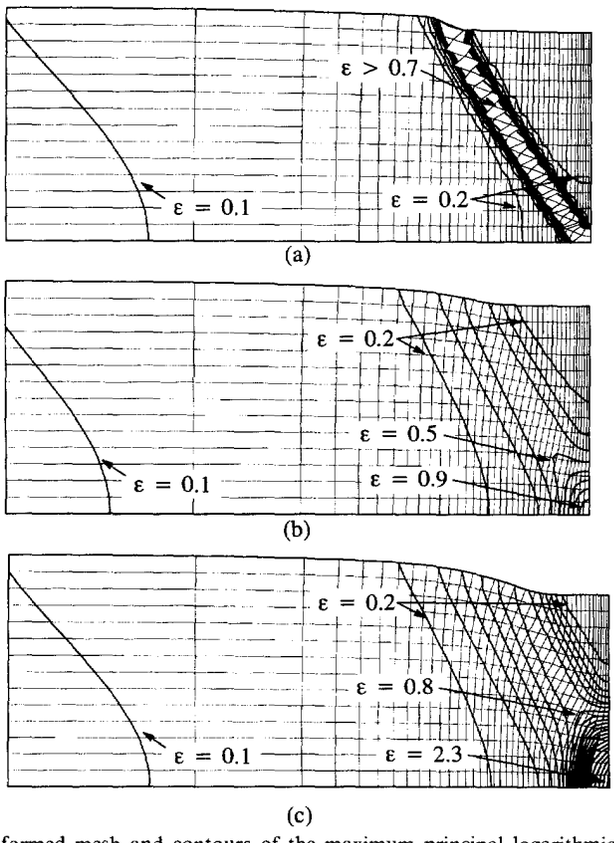

Fig. 8. The deformed mesh and contours of the maximum principal logarithmic strain for the analyzed part of a sheet under uniaxial tension with $A_0/B_0 = 2$, $B_0/H_0 = 16$, $\bar{\xi} = 0.001$, $\phi = 0$, $\sigma_0/E = 0.0033$, $n = 10$ and $\nu = 0.3$. (a) Local J_2-flow theory at $\varepsilon_a = 0.163$. (b–c) Gradient dependent J_2-flow theory with $g(\lambda) = \ell^2\sigma_y(\lambda)$, $\ell = 0.243H$ at (b) $\varepsilon_a = 0.163$ and (c) $\varepsilon_a = 0.197$.

the Considére (1885) condition, first onset of localization shows only a small delay compared to the maximum load point for both models. This is due to the fact that the aspect ratio ($A_0/B_0 = 2$) is sufficiently large. The critical strain for bifurcation in the localized oblique neck is much larger than that at the load maximum and, therefore, the localized necks occur as a secondary instability in the diffuse neck region, well after the first onset of necking, Tvergaard (1993). The width of the oblique neck for the gradient dependent model is given by the incorporated length and is, thereby, related to the current thickness of the sheet. For the local 2-D plasticity model ($\ell = 0$) the oblique localized neck results from loss of ellipticity of the governing equations, but in the non-local 2-D model the problem remains elliptic (see for example Benallal and Tvergaard, 1995).

Figures 8(a, b) show the deformed mesh and the contours of the maximum principal logarithmic strain for the local and the gradient dependent models, respectively, at an elongation corresponding to $\varepsilon_a = 0.163$. For the local plasticity theory (Fig. 8(a)), the width of the necking zone is seen to be given by the size of the elements in the necking zone, where only one or two rows of elements are strongly deformed. Therefore, the post-necking behaviour for a 2-D local plasticity model is strongly mesh dependent. This is not the case for the gradient dependent model (Fig. 8(b)), where the width of the necking zone is solely given by the incorporated length scale.

Except for an insignificant difference in the hardening rule (6), the specimen analyzed (Figs 7–8) is exactly the same as the specimen analyzed by an accurate full numerical (3-D) local plasticity analysis in Tvergaard (1993). A reasonable agreement between the contours in Figs 8(b, c) for the 2-D gradient dependent model and the results in Tvergaard (1993) is obtained. As expected from the increasing difference of the post-necking load-deformation paths for increasing stretching (Fig. 6), the best agreement is found in Fig. 8(b). The maximum principal logarithmic strain in the center of the necking zone has not

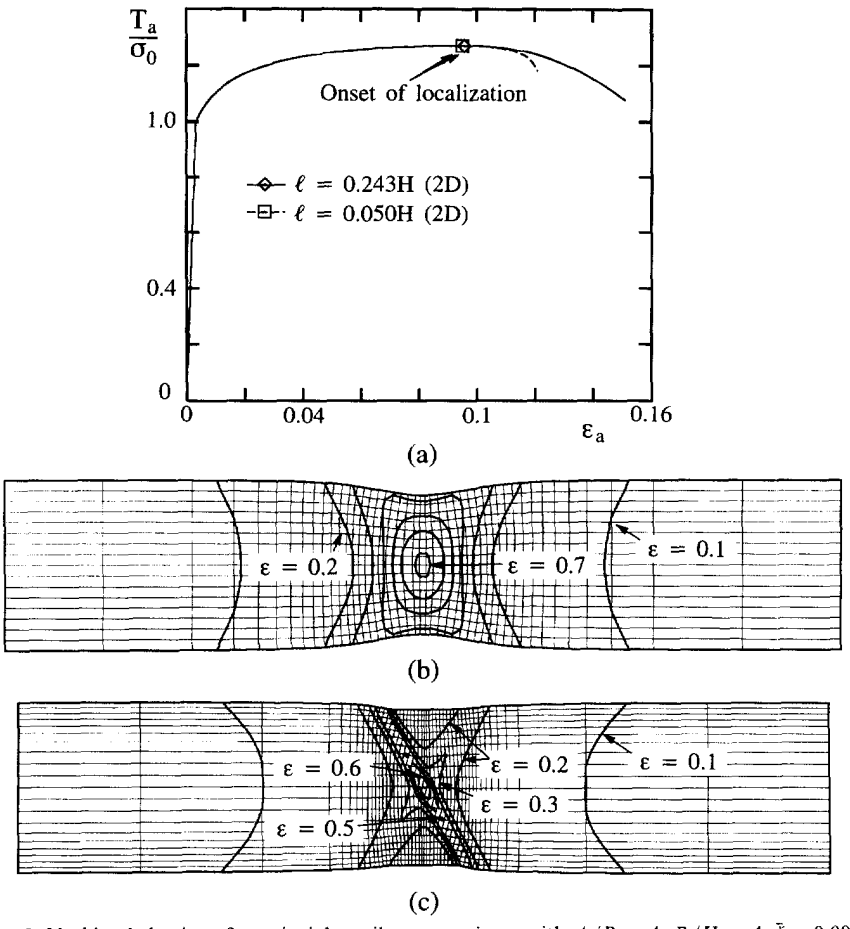

Fig. 9. Necking behaviour for uniaxial tensile test specimen with $A_0/B_0 = 4$, $B_0/H_0 = 4$, $\bar{\xi} = 0.001$, $\phi = 2.9°$, $\sigma_0/E = 0.0033$, $n = 10$ and $\nu = 0.3$. (a) Average nominal traction vs the average longitudinal strain for a gradient dependent plasticity theory ($g(\lambda) = \ell^2\sigma_y(\lambda)$) with two different incorporated length scale. (b–c) The deformed mesh and contours of the maximum principal logarithmic strain at $H_{min}/H_0 = 0.652$ for (b) $\ell = 0.243H$ and (c) $\ell = 0.050H$.

reached as high values in Fig. 8(c) as in Tvergaard (1993) [$0.7 < \varepsilon < 0.8$ in Fig. 8(c) compared to $0.9 < \varepsilon < 1.0$ in Tvergaard (1993)] and the width of the necking zone is somewhat larger here. Remark, that the elongation corresponding to $\varepsilon_a = 0.197$, is so large that the sheet thickness locally is very thin ($H_{min} = 0.11H_0$), which also results in very deformed elements (lower right corner in Fig. 8(c)).

Due to the symmetry boundary conditions, the necking band shown in Figs 8(a–c) corresponds to two crossing necking bands in the uniaxial tensile specimen (Fig. 1). If instead the whole specimen is analyzed with a little inclination $\phi \neq 0$ of the imperfection (19), only one of the two necks will continue to develop at an early stage in the post-necking region, see Tvergaard (1993). In Fig. 9 a tensile test specimen ($A_0/B_0 = 4$ and $B_0/H_0 = 4$) with an initial imperfection (19) given by $\bar{\xi} = 0.001$ and $\phi = 2.9°$ is analyzed by a 2-D gradient dependent model with $g(\lambda) = \ell^2\sigma_y(\lambda)$. The post-necking behaviour is compared for two different incorporated length scale ($\ell = 0.243H$ and $\ell = 0.050H$).

The incorporated length $\ell = 0.243H$ gives no inclination of the necking zone in Fig. 9(b), which corresponds to the post-necking behaviour of a thick sheet (Tvergaard, 1993). An inclination of the necking zone requires a sufficiently smaller length scale, $\ell = 0.050H$ (Fig. 9(c)). A few calculations with a coarser mesh have been carried out to guarantee that the post-necking behaviour is still solely determined by the incorporated length scale and not by the mesh.

Figure 10 shows the corresponding comparison between the 1-D gradient dependent model and the 2-D full numerical model. Figure 10(a) shows the softer post-necking

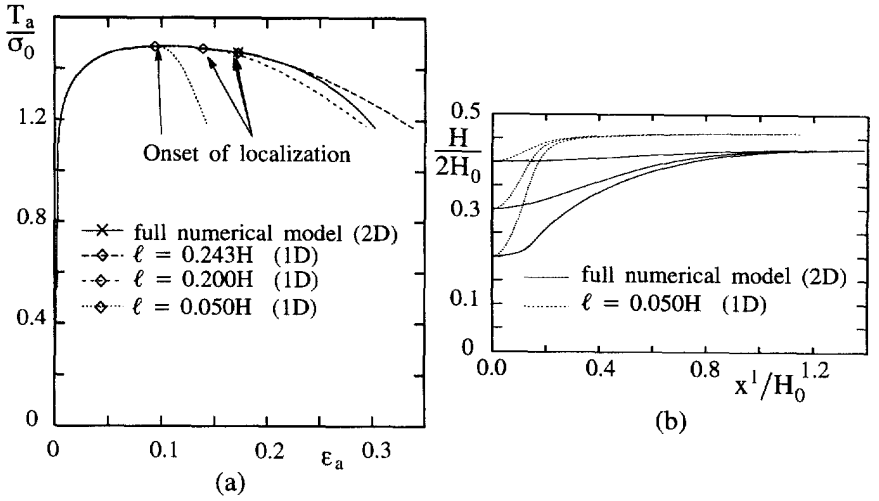

Fig. 10. Necking behaviour for a plane strain tensile test with $A_0/H_0 = 2$, $\bar{\xi} = 0.001$, $\phi = 0$, $\sigma_0/E = 0.0033$, $n = 3$ and $\nu = 0.3$. (a) The average nominal traction vs the average longitudinal strain for a full 2-D plane strain analysis and a gradient dependent plasticity theory ($g(\lambda) = \ell^2\sigma_y(\lambda)$) with two different incorporated length scales. (b) Thickness variation at three different deformation state ($H_{\min} = 0.8H_0$, $H_{\min} = 0.6H_0$ and $H_{\min} = 0.4H_0$) for the full (2-D) model and the gradient dependent (1-D) model with $\ell = 0.050H$.

behaviour for the incorporated length $\ell = 0.050H$ and the corresponding thickness variation is shown in Fig. 10(b), where also a smaller neck width is observed. A comparison of Fig. 9(c) with Tvergaard (1993) shows also that the width of the necking zone predicted by the gradient dependent model is too small. A larger incorporated length, on the other hand, will not result in an inclination of the necking zone. Thus, a length $\ell = 0.100H$ will result in a post-necking zone of two crossing neck bands, where it is rather late in the post-necking regime ($H_{\min} < 0.3H_0$) that one of the neck bands begins to develop faster than the other. One possible explanation of this larger delay is that the 3-D solution in Tvergaard (1993) might include some mesh effects due to the use of an inclined concentrated mesh. In the present gradient dependent analysis such an inclined concentrated mesh cannot be tested because of the requirement of rectangular elements.

5.4. *Laplacian taken with respect to the current deformed state*

In the analysis presented above, the Laplacian is taken with respect to the undeformed reference state ($\nabla_0^2\lambda = \lambda_{,ii}$). An alternative is to take the Laplacian with respect to the current state. In the Lagrangian convected coordinate formulation, the Laplacian for a plane stress assumption will then have the following form

$$\nabla^2\lambda = G^{\alpha\beta}_{,\alpha}\lambda_{,\beta} + G^{\alpha\beta}\lambda_{,\alpha\beta} \tag{20}$$

with $G^{\alpha\beta}_{,\alpha} = -2G^{\alpha\gamma}G^{\delta\beta}\eta_{\gamma\delta,\alpha}$ (Spiegel, 1959). The increment of the Laplacian is given by

$$(\nabla^2\lambda)^{\cdot} = \dot{G}^{\alpha\beta}_{,\alpha}\lambda_{,\beta} + G^{\alpha\beta}_{,\alpha}\dot{\lambda}_{,\beta} + \dot{G}^{\alpha\beta}\lambda_{,\alpha\beta} + G^{\alpha\beta}\dot{\lambda}_{,\alpha\beta} \tag{21}$$

where $\dot{G}^{\alpha\beta}_{,\alpha}$ is given by

$$\dot{G}^{\alpha\beta}_{,\alpha} = -2(\dot{G}^{\alpha\gamma}G^{\delta\beta}\eta_{\gamma\delta,\alpha} + G^{\alpha\gamma}\dot{G}^{\delta\beta}\eta_{\gamma\delta,\alpha} + G^{\alpha\gamma}G^{\delta\beta}\dot{\eta}_{\gamma\delta,\alpha}) \tag{22}$$

with $\dot{G}^{\alpha\gamma} = -2G^{\alpha\beta}G^{\delta\gamma}\dot{\eta}_{\beta\delta}$.

The expressions for the Laplacian with respect to the current state contain terms with $\eta_{\gamma\delta,\alpha}$ and $\dot{\eta}_{\gamma\delta,\alpha}$. Therefore, the Laplacian of the plastic multiplier λ depends now also on the second derivative of the displacement u_α and the increments thereof. A C^0-compatible isoparametric approximation of the displacements is, therefore, no longer sufficient, and

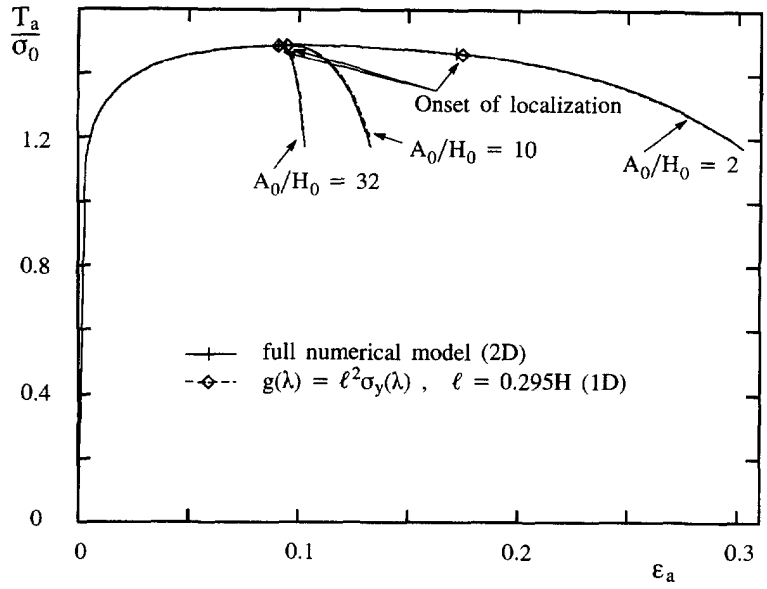

Fig. 11. The average nominal traction vs the average longitudinal strain for a specimen with $\bar{\xi} = 0.001$, $\phi = 0$, $\sigma_0/E = 0.0033$, $n = 10$ and $\nu = 0.3$. The Laplacian in the gradient dependent model is taken with respect to the current configuration $[\nabla^2\lambda = (G^{ij}\lambda_{,i})_{,j}]$.

now also the modeling of the displacements requires a C^1-compatible modeling. In the following, both the increment of the plastic multiplier $\dot{\lambda}$ and the increment of the displacement $\dot{u}_\alpha$ are modelled in terms of four-noded rectangular elements with Hermitian cubics. A 2×2 Gauss integration scheme, as used above, does not suffice, as this gives a singular solution. Instead a 3×3 Gauss integration scheme is used, despite the fact that for the case of the combined isoparametric/Hermitian elements some oscillations of the values have been observed in the 3×3 Gauss integration points, see also Pamin (1994).

The computations are carried out for the case of plane strain, as in Section 5.2. Figure 11 shows the exact (2-D plane strain) solution along with a gradient dependent solution where the Laplacian of the plastic multiplier is taken with respect to the current deformation state. Due to the oscillations of the value of the yield function f (eqn (10)) in the integration points (with 3×3 integration), it is not possible to constrain the solution to satisfy requirement $f \leqslant 10^{-3}\sigma_0$ during plastic yielding. Instead it is necessary to allow the solution to differ up to $f \leqslant 0.02\sigma_0$ from the yield surface in some integration points in some areas in the solution history. On the other hand, the agreement between the exact and the approximate (gradient dependent) solution is very good. Both with respect to the delay of the onset of localization and the post-necking behaviour. This result is found for an incorporated length scale of $\ell = 0.295H$, where H is the current thickness.

Figure 12 shows the corresponding thickness variation in the axial direction for the most stocky specimen. Here a nice agreement is also found, but the gradient dependent model has a tendency to localize slightly more. A slightly larger incorporated length ($\ell = 0.3H$) gives a better fit of the thickness variation, but then the load deflection curve is slightly too stiff, i.e. 1–2% too high load for a given strain in the post-necking zone.

A 2-D gradient dependent finite element analysis for a strip under uniaxial tension, leading to inclined necks as in Figs 7–9, has been carried out. However, here the oscillations of the values in the integration points grew too large. Improved algorithm for this case will be studied in a subsequent paper.

6. CONCLUSION

The post-necking behaviour for stretched thin sheets has been modeled by a non-local continuum model, which is here a finite strain version of a gradient dependent J_2-flow theory. Using this enhanced model, it has been demonstrated how it is possible to find a mesh

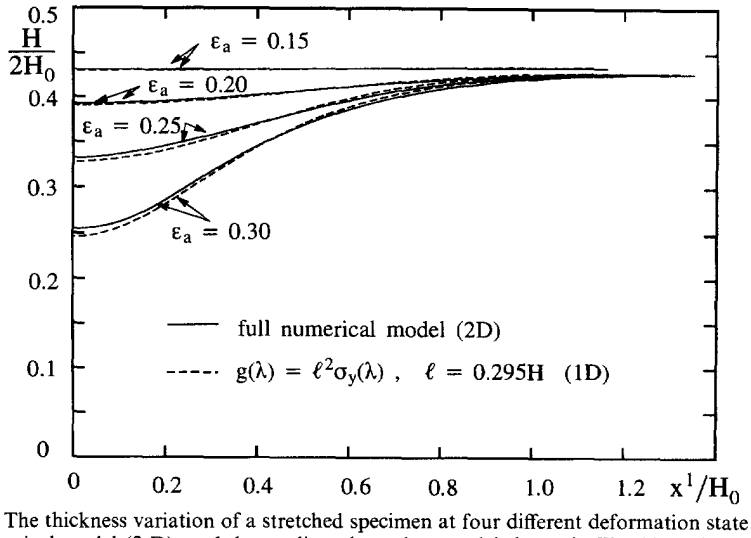

Fig. 12. The thickness variation of a stretched specimen at four different deformation state for the full numerical model (2-D), and the gradient dependent model shown in Fig. 11. with $A_0/H_0 = 2$, $\bar{\xi} = 0.001$, $\phi = 0$, $\sigma_0/E = 0.0033$, $n = 10$ and $\nu = 0.3$. The Laplacian in the gradient dependent model is taken with respect to the current configuration [$\nabla^2\lambda = (G^{ij}\lambda_{,i})_{,j}$].

independent post-necking behaviour based on a plane stress model. For the corresponding classical (local) plasticity theory this would require a full 3-D numerical finite element model. Also, it has been shown how the delay of the onset of localization in the imperfect stretched sheet is governed by the incorporated length scale in the gradient dependent J_2-flow theory.

The applicability of the plane stress gradient dependent model is evaluated by numerical comparison with the corresponding classical (local) model, taking into full account of 3-D effects. For the simplest modeling of the Laplacian of the effective plastic strain in the enhanced model (with respect to the undeformed reference configuration) a reasonable agreement with the full numerical model has been obtained, with the best agreement in cases where the length scale is normalized with respect to the current thickness of the deformed sheet. The difference in the post-necking region is found to increase, where the downward curvature of the load vs stretch curve for the enhanced model is too small compared to the full 3-D numerical model.

The approximation in the post-necking regime can be improved by choosing a more complicated model of the Laplacian, where the Laplacian is taken with respect to the current deformation state of the stretched sheet. This brings the second derivative of the displacements into the governing equations, causing some trouble in the numerical method where the integration points in the model oscillate. Despite this difficulty, a very nice agreement between the 1-D gradient dependent model and the 2-D full numerical solution is obtained.

The transition between the usual diffuse necking mode in a tensile test specimen and the localized oblique sheet necking mode has been analyzed by a 2-D gradient dependent model for a strip under uniaxial tension (Fig. 9). The dependence of the final dominant necking mode to the cross-section aspect ratio (B_0/H_0) is demonstrated, where a large incorporated length ℓ in Fig. 9 represents a relatively small cross-section aspect ratio. Based on the corresponding classical plasticity analysis this dependency cannot be determined by a plane stress analysis, but requires a full 3-D finite element model, Tvergaard (1993).

Acknowledgement—The author wishes to thank Professor Viggo Tvergaard at the Technical University of Denmark for many valuable discussions during the course of this work. Financial support by the MUP2 research programme Materials Processing, Properties and Modeling, financed by the Danish Agency for Development of Trade and Industry, the Danish Natural Science Research Council, and the Danish Technical Research Council is gratefully acknowledged.

REFERENCES

Aifantis, E. C. (1984). On the microstructural origin of certain inelastic models. *Transactions of the ASME Journal of Engineering Material Technology*, **106,** 326–330.

Aifantis, E. C. (1987). The physics of plastic deformation. *International Journal of Plasticity*, **3,** 211–247.

Benallal, A. and Tvergaard, V. (1995). Non-local continuum effects on bifurcation in the plane strain tension-compression test. *Journal of Mechanics and Physics of Solids*, **43,** 741–770.

de Borst, R. and Mühlhaus, H.-B. (1992). Gradient-dependent plasticity: formulation and algorithmic aspects. *International Journal for Numerical Methods in Engineering*, **35,** 521–539.

Budiansky, B. (1969). Remarks on theories of solid and structural mechanics. In *Problems of Hydrodynamics and Continuum Mechanics*, eds M. A. Lavrent'ev *et al.*, pp. 77–83. SIAM, Philadelphia.

Considére, M. (1885). *Annales des Ponts et Chausseés*, **9,** 574.

Eringen, A. C. (1968). Theory of micropolar elasticity. *Fracture, an advanced Treatise*, ed. H. Leibowitz, pp. 621–729. Academic Press, New York.

Fleck, N. A. and Hutchinson, J. W. (1993). A phenomenological theory of strain gradient plasticity. *Journal of Mechanics and Physics of Solids*, **41,** 1825–1857.

Fleck, N. A. and Hutchinson, J. W. (1996). Strain gradient plasticity. *Advances in Applied Mechanics*, **33,** 295–361.

Hill, R. and Hutchinson, J. W. (1975). Bifurcation phenomena in the plane tension test. *International Journal of Solids Structures*, **23,** 239–264.

Hutchinson, J. W. (1973). Finite strain analysis of elastic–plastic solids and structures. In *Numerical Solution of Nonlinear Structural Problems*, ed. R. F. Hartung, p. 17. ASME, New York.

Keeler, S. P. (1968). Understanding sheet metal formability. *Machinery and Production Engineering*, Part 1–6.

Mikkelsen, L. P. (1996). Necking of biaxially stretched thin sheets modeled by a nonlocal plasticity theory. In *Proc. of the 3rd Asia–Pacific Symposium on Advances in Engineering Plasticity and its Applications*, eds. T. Abe and T. Tsuta, pp. 579–584. Pergamon Elsevier, Hiroshima.

Mühlhaus, H.-B. and Aifantis, E. C. (1991). A variational principle for gradient plasticity. *International Journal of Solids Structures*, **28,** 845–856.

Mühlhaus, H.-B. and Vardoulakis, I. (1987). The thickness of shear bands in granular materials. *Géotechnique*, **37,** 271–283.

Pamin, J. (1994). Gradient-dependent plasticity in numerical simulation of localization phenomena. Dissertation, Delft University of Technology, Delft.

Pamin, J. and de Borst, R. (1995). Numerical simulation of localization phenomena using gradient plasticity and finite elements. In *Heron, Netherlands School for Advanced Studies in Construction*, ed. A. C. W. M. Vrouwenvelder, Vol. 40, pp. 71–92. Delft, The Netherlands.

Pijaudier-Cabot, G. and Bazant, Z. P. (1987). Nonlocal damage theory. *Journal of Engineering Mechanics ASCE*, **113,** 1512–1533.

Spiegel, M. R. (1959). *Theory and Problems of Vector Analysis and an Introduction to Tensor Analysis*. Schaum, New York.

Tvergaard, V. (1981). Bifurcation and imperfection—sensitivity at necking instabilities. *ZAMM*, **60,** T26–T34.

Tvergaard, V. (1993). Necking in tensile bars with rectangular cross-section. *Computing Methods in Applied Mechanics and Engineering*, **103,** 273–290.